



Cite this: *Mater. Horiz.*, 2024,  
11, 6049Received 5th June 2024,  
Accepted 12th September 2024

DOI: 10.1039/d4mh00715h

rsc.li/materials-horizons

Design principle of disordered rocksalt type  
overlithiated anode for high energy density  
batteries†Yufang He,  Zhengda He and Bin Ouyang  \*

Rechargeable lithium-ion batteries with high energy density and fast-charging capability are vital for commercial applications. Disordered rocksalt (DRX) materials with a cation/anion ratio greater than one, achieved through additional lithium insertion, have emerged as promising high-rate anode candidates. Inspired by the previously reported  $\text{Li}_{3+x}\text{V}_2\text{O}_5$  ( $0 \leq x \leq 2$ ) anode, a comprehensive search was conducted for all potential redox centers using high-throughput density functional theory (DFT) computations. This study examined 23 redox centers in a prototype formula  $\text{Li}_{3+x}\text{V}_2\text{O}_5$  ( $0 \leq x \leq 2$ ) with the DRX structure, analyzing aspects such as voltage curve, theoretical capacity, energy density, phase stability, electronic conductivity, and volumetric change during cycling. Promising candidates were identified with redox centers including V, Cr, Nb, Mn, and Fe, marking them as potential anode materials. Additionally, this research revealed the origin of the low voltage in DRX anodes and proposed a method to optimize the average voltage by tuning the relative energies among structures with varying lithium contents. This work provides compositional design principles for the new promising DRX anode of LIBs with high energy density, fast-charging capability, and good cycling stability.

## Introduction

Rechargeable lithium-ion batteries (LIBs) with high energy density, fast-charging capability, cycling stability, and safety are required to satisfy the increasing global energy demand.<sup>1–5</sup> The disordered rock-salt (DRX) oxides recently emerged as promising intercalation anodes.<sup>6–10</sup> The lower lithium-ion intercalation voltage of the DRX anode contributes to the higher energy density of LIBs.<sup>6,8,11,12</sup> Recently, DRX  $\text{Li}_{3+x}\text{V}_2\text{O}_5$  ( $0 \leq x \leq 2$ )<sup>6</sup> has been reported as a promising DRX anode with an average

## New concepts

We introduced a new concept for estimating the average voltage of a broad range of Li-ion battery anode materials. This concept uses the relative energy between the overlithiated state and the stoichiometric state. It applies to materials with a cation/anion ratio larger than one and a disordered rocksalt (DRX) structure. The concept is based on about 7680 density functional theory calculations across 23 metals and 13Li contents per formula unit. Additionally, we have identified ten material systems that outperform the state-of-the-art Lithium Titanate commercialized anode. Given the vast design space of overlithiated DRX materials, this concept will significantly accelerate the discovery of novel intercalation electrodes.

intercalation voltage of 0.58 V. Such anodes in general operate at the composition with cation/anion ratio larger than 1.0, which is referred to as overlithiated DRX.<sup>13</sup> As a result of overlithiation, the lithium-ion diffusivity will be greatly enhanced, which leads to extraordinary rate performance for fast charging applications.<sup>6,14</sup> The origin of high ionic conductivity stems from the face-sharing local structures that are enforced by overlithiation,<sup>8,13,14</sup> which is the key to high lithium-ion diffusivity in several cases even without overlithiation.<sup>15,16</sup>

Understanding overlithiated disordered rock-salt (DRX) compounds is essential, as DRX-type  $\text{Li}_{3+x}\text{V}_2\text{O}_5$  has demonstrated reversible cycling between 0.01 V and 2 V with a specific capacity of  $\sim 255 \text{ mAh g}^{-1}$ .<sup>6</sup> This material exhibits excellent rate capability and maintains stable performance over 1000 charge-discharge cycles with negligible capacity decay, leading to its recent commercialization. Additionally, our recent computational and experimental work<sup>13</sup> has confirmed that various overlithiated DRX compounds can be directly synthesized through the solid-state synthesis method. Therefore, it reveals that there is an overlooked potential of the overlithiated DRX compounds.

Given the promises for building DRX anodes with overlithiation composition design, the viable chemical space is still largely unknown. In this work, 23 redox centers (e.g. Ti, V, Cr, Mn, Fe, Co, Ni, Cu, Ge, Zr, Nb, Mo, Rh, Ru, Sn, Sb, Te, Hf, Ta,

Department of Chemistry and Biochemistry, Florida State University, Tallahassee, FL 32304, USA. E-mail: yh23m@fsu.edu, zh23b@fsu.edu, bouyang@fsu.edu

† Electronic supplementary information (ESI) available: The supplementary information document and the original data of all DRX anode materials calculations are available online. See DOI: <https://doi.org/10.1039/d4mh00715h>

W, Re, Ir, Ce) were thoroughly evaluated concerning the possibility of acting as promising anode materials when intercalating from  $\text{Li}_3\text{M}_2\text{O}_5$  to  $\text{Li}_5\text{M}_2\text{O}_5$ . For each redox center, the average voltage, theoretical capacity, and energy density of 23 systems are calculated by even sample of Li content ranging from 3Li per  $\text{O}_5$  ( $\text{Li}_3\text{M}_2\text{O}_5$ ) to 5Li per  $\text{O}_5$  Li ( $\text{Li}_5\text{M}_2\text{O}_5$ ) and at least 16 types of different ordered structures are sampled for each Li content. Taking  $\text{Li}_{4+x}\text{Ti}_5\text{O}_{12}$  (LTO) ( $0 \leq x \leq 3$ )<sup>15</sup> as a reference, there are some promising anode materials with similar or higher energy densities. Among these, several new anode compositions are presented that are comparable to or better than state-of-art  $\text{Li}_{3+x}\text{V}_2\text{O}_5$  ( $0 \leq x \leq 2$ )<sup>6</sup> in terms of performance, stability, volumetric change, cost, and electronic conductivity. Additionally, the voltage curves of selected low voltage and high voltage DRX  $\text{Li}_{3+x}\text{M}_2\text{O}_5$  anode are presented. Furthermore, we also established a straightforward way to understand the origin and tunability of average voltage for overlithiated DRX anodes.

## Results and discussion

High energy density anode is a crucial requirement for the next generation of LIBs.<sup>17–20</sup> DRX anode has been regarded as a high energy density anode due to its high theoretical capacity and low voltage.<sup>6,7</sup> To discover more promising DRX anodes with high energy density and find the fundamental mechanism of high-performance overlithiated DRX anode, 23 redox centers, Ti, V, Cr, Mn, Fe, Co, Ni, Cu, Ge, Zr, Nb, Mo, Rh, Ru, Sn, Sb, Te, Hf, Ta, W, Re, Ir, and Ce, were systematically evaluated when lithium-ion intercalation from  $\text{Li}_3\text{M}_2\text{O}_5$  to  $\text{Li}_5\text{M}_2\text{O}_5$ . The typical structure of  $\text{Li}_{3+x}\text{M}_2\text{O}_5$  is demonstrated in Fig. 1(a), the extra Li is assumed to be inserted into the tetrahedron sites according to previous reports.<sup>6,13</sup> Building on the DFT computed average voltage and capacity, the Ragone plot<sup>21–23</sup> that correlates theoretical capacity and average voltage with energy density is shown in Fig. 1(b). The average voltage of the cathode is assumed to be 4 V in the calculations, which is achievable in state-of-the-art Ni-rich cathodes.<sup>6,24,25</sup> Compared with the reported LTO<sup>15</sup> with a theoretical capacity of

175.14  $\text{mAh g}^{-1}$  and average voltage of 1.55 V, the theoretical capacity of 11 DRX  $\text{Li}_{3+x}\text{M}_2\text{O}_5$  compounds (where  $\text{M} = \text{Cu}, \text{Ni}, \text{Co}, \text{Fe}, \text{Ge}, \text{Mn}, \text{Cr}, \text{Ru}, \text{Rh}, \text{V}$ , and  $\text{Nb}$ ) are higher.<sup>15</sup> Among those promising candidates, Mn, Cr, Nb, and V-based anodes stand out among all candidates with the highest energy densities ( $> 600 \text{ Wh kg}^{-1}$ ). Particularly, V shows the highest theoretical capacity of 264.44  $\text{mAh g}^{-1}$  and energy density of 930.22  $\text{Wh kg}^{-1}$  respectively (Table S1, ESI†). The calculated theoretical capacity of 264.44  $\text{mAh g}^{-1}$  is close to the experimentally measured capacity value of  $\sim 255 \text{ mAh g}^{-1}$ .<sup>6</sup> While Nb shows the lowest theoretical accessible voltage as 0.19 V, even though the energy density is relatively lower at 711.60  $\text{Wh kg}^{-1}$  due to the much larger molar mass of Nb. Moreover, Ru, Rh, Ge, Fe, and Mn also show larger energy density compared with reported LTO, with energy densities being 535.21  $\text{Wh kg}^{-1}$ , 469.17  $\text{Wh kg}^{-1}$ , 527.79  $\text{Wh kg}^{-1}$ , 519.74  $\text{Wh kg}^{-1}$ , and 663.02  $\text{Wh kg}^{-1}$  respectively. Additionally,  $\text{Li}_{3+x}\text{M}_2\text{O}_5$  compounds that contain Sn, Co, Ni, and Sb are very close to the energy density of the LTO anode. Nevertheless,  $\text{Li}_{3+x}\text{M}_2\text{O}_5$  compounds with certain metals, *e.g.* Mo, W, and Ce also display very competitive voltage with limited capacity. On the other hand, Ti, Zr, Hf, and Ta-based  $\text{Li}_{3+x}\text{M}_2\text{O}_5$  turn out to be electrochemically inactive at all.

A promising anode material for lithium-ion batteries (LIBs) should ideally have a near-zero low intercalation voltage to maximize energy density. Consequently, the voltage curves of various DRX anode materials are analyzed through high-throughput screening of density functional theory (DFT) data. The analysis focuses on understanding the low voltage characteristics of DRX  $\text{Li}_{3+x}\text{M}_2\text{O}_5$  materials. The selected voltage curves are depicted in Fig. 2, organized by the magnitude of the average voltage. Specifically, Fig. 2(a) showcases candidates with voltages close to 0 V, including materials with M as Ce, Re, Nb, V, Ru, and Cr, while Fig. 2(b) features candidates with average voltages above 1.5 V, comprising materials with M as Cu, Ni, Co, Fe, Te, and Sb. The average voltages for these selected low and high-voltage DRX  $\text{Li}_{3+x}\text{M}_2\text{O}_5$  ( $\text{M} = \text{Ce}, \text{Re}, \text{Nb}, \text{V}, \text{Ru}, \text{Cr}, \text{Cu}, \text{Ni}, \text{Co}, \text{Fe}, \text{Te}$ , and  $\text{Sb}$ ) are as follows:

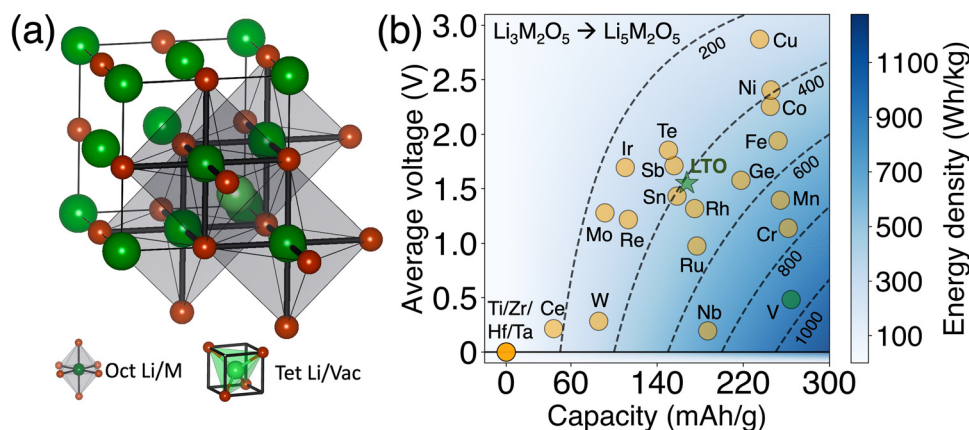
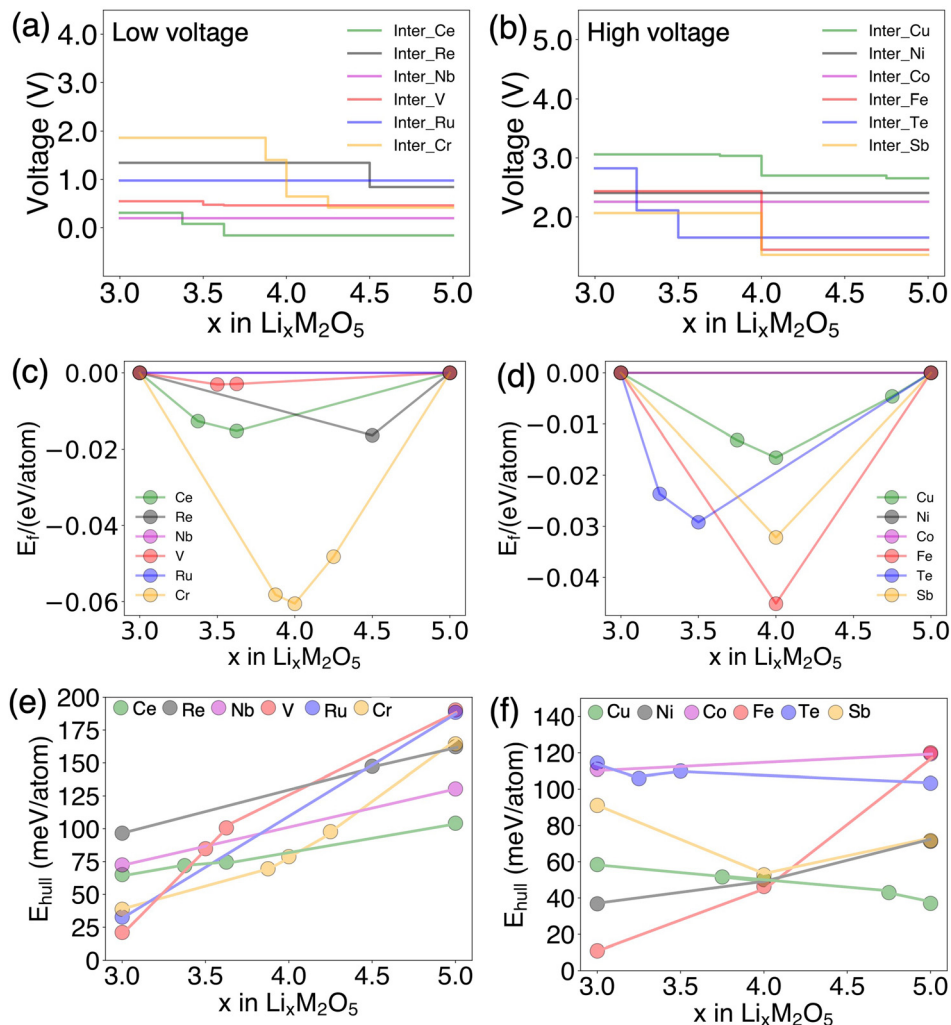


Fig. 1 Overview of high throughput screening DFT data: (a) the atomic structure of  $\text{Li}_{3+x}\text{M}_2\text{O}_5$  ( $0 \leq x \leq 2$ ); (b) Ragone plot of the average voltage, theoretical capacity, and energy density of all searched DRX  $\text{Li}_{3+x}\text{M}_2\text{O}_5$  ( $0 \leq x \leq 2$ ) ( $\text{M} = \text{Ti}, \text{V}, \text{Cr}, \text{Mn}, \text{Fe}, \text{Co}, \text{Ni}, \text{Cu}, \text{Ge}, \text{Zr}, \text{Nb}, \text{Mo}, \text{Rh}, \text{Ru}, \text{Sn}, \text{Sb}, \text{Te}, \text{Hf}, \text{Ta}, \text{W}, \text{Re}, \text{Ir}, \text{Ce}$ ) and reported  $\text{Li}_{4+x}\text{Ti}_5\text{O}_{12}$  ( $0 \leq x \leq 3$ ).<sup>15</sup>





**Fig. 2** Analysis of selected compounds with low voltage and high voltage: (a) the voltage curve of  $\text{Li}_{3+x}\text{M}_2\text{O}_5$  with relative low average voltage ( $\text{M} = \text{Ce}$ ,  $\text{Re}$ ,  $\text{Nb}$ ,  $\text{V}$ ,  $\text{Ru}$ , and  $\text{Cr}$ ); (b) the voltage curve of  $\text{Li}_{3+x}\text{M}_2\text{O}_5$  with relative high average voltage ( $\text{M} = \text{Cu}$ ,  $\text{Ni}$ ,  $\text{Co}$ ,  $\text{Fe}$ ,  $\text{Te}$ , and  $\text{Sb}$ ); (c) and (d) the intercalation convex hull of selected low and high voltage DRX  $\text{Li}_{3+x}\text{M}_2\text{O}_5$  ( $\text{M} = \text{Ce}$ ,  $\text{Re}$ ,  $\text{Nb}$ ,  $\text{V}$ ,  $\text{Ru}$ ,  $\text{Cr}$ ,  $\text{Cu}$ ,  $\text{Ni}$ ,  $\text{Co}$ ,  $\text{Fe}$ ,  $\text{Te}$ , and  $\text{Sb}$ ); (e) and (f) the stability ( $E_{\text{hull}}$ ) of selected low and high voltage DRX  $\text{Li}_{3+x}\text{M}_2\text{O}_5$  ( $\text{M} = \text{Ce}$ ,  $\text{Re}$ ,  $\text{Nb}$ ,  $\text{V}$ ,  $\text{Ru}$ ,  $\text{Cr}$ ,  $\text{Cu}$ ,  $\text{Ni}$ ,  $\text{Co}$ ,  $\text{Fe}$ ,  $\text{Te}$ , and  $\text{Sb}$ ).

0.21 V, 1.22 V, 0.19 V, 0.48 V, 0.98 V, 1.14 V, 2.87 V, 2.41 V, 2.26 V, 1.94 V, 1.85 V, and 1.71 V respectively, as listed in Table S1 (ESI<sup>†</sup>). Additionally, the intercalation voltage curves for other DRX  $\text{Li}_{3+x}\text{M}_2\text{O}_5$  materials not included in Fig. 2 ( $\text{M} = \text{Ti}$ ,  $\text{Mn}$ ,  $\text{Ge}$ ,  $\text{Zr}$ ,  $\text{Rh}$ ,  $\text{Sn}$ ,  $\text{Hf}$ ,  $\text{Ta}$ ,  $\text{W}$ ,  $\text{Ir}$ , and  $\text{Mo}$ ) are presented in Fig. S1 (ESI<sup>†</sup>). Among all examined DRX  $\text{Li}_{3+x}\text{M}_2\text{O}_5$  materials, DRX  $\text{Li}_{3+x}\text{Nb}_2\text{O}_5$  exhibits the lowest voltage, and the intercalation voltage for all DRX anode materials decreases during the lithiation process.

To further study the stability of DRX  $\text{Li}_{3+x}\text{M}_2\text{O}_5$  ( $0 \leq x \leq 2$ ) anode during lithiation, the intercalation convex hull of all searched DRX  $\text{Li}_{3+x}\text{M}_2\text{O}_5$  ( $\text{M} = \text{Ti}$ ,  $\text{V}$ ,  $\text{Cr}$ ,  $\text{Mn}$ ,  $\text{Fe}$ ,  $\text{Co}$ ,  $\text{Ni}$ ,  $\text{Cu}$ ,  $\text{Ge}$ ,  $\text{Zr}$ ,  $\text{Nb}$ ,  $\text{Mo}$ ,  $\text{Rh}$ ,  $\text{Ru}$ ,  $\text{Sn}$ ,  $\text{Sb}$ ,  $\text{Te}$ ,  $\text{Hf}$ ,  $\text{Ta}$ ,  $\text{W}$ ,  $\text{Re}$ ,  $\text{Ir}$ , and  $\text{Ce}$ ) anodes are calculated (Fig. 2c and d and Fig. S2, ESI<sup>†</sup>). Fig. 2(c) and (d) shows the intercalation convex hull of selected low voltage  $\text{Li}_{3+x}\text{M}_2\text{O}_5$  ( $\text{M} = \text{Ce}$ ,  $\text{Re}$ ,  $\text{Nb}$ ,  $\text{V}$ ,  $\text{Ru}$ ,  $\text{Cr}$ ) and high voltage  $\text{Li}_{3+x}\text{M}_2\text{O}_5$  ( $\text{M} = \text{Cu}$ ,  $\text{Ni}$ ,  $\text{Co}$ ,  $\text{Fe}$ ,  $\text{Te}$ , and  $\text{Sb}$ ). The more complete convex hull with metastable compounds is shown in Fig. S3

(ESI<sup>†</sup>). Cr compounds feature the deepest convex hull around  $x = 4.0$ , followed by Re and Ce in Fig. 2(c). On the other hand, Ru and Nb have a flat intercalation hull, which leads to no step as shown in the voltage curve of Fig. 2(a). It is also noted that the  $E_{\text{hull}}$  values do not necessarily form a convex hull, particularly for DRX  $\text{Li}_{3+x}\text{Ce}_2\text{O}_5$ ,  $\text{Li}_{3+x}\text{V}_2\text{O}_5$ ,  $\text{Li}_{3+x}\text{Cu}_2\text{O}_5$ , and  $\text{Li}_{3+x}\text{Te}_2\text{O}_5$  systems. This is owing to the variation of competing phases during the intercalation process, which can be further supported by Fig. S4–S6 (ESI<sup>†</sup>).

Furthermore, the energy above hull ( $E_{\text{hull}}$ ) of selected low voltage DRX  $\text{Li}_{3+x}\text{M}_2\text{O}_5$  ( $\text{M} = \text{Ce}$ ,  $\text{Re}$ ,  $\text{Nb}$ ,  $\text{V}$ ,  $\text{Ru}$ ,  $\text{Cr}$ ) and high voltage DRX  $\text{Li}_{3+x}\text{M}_2\text{O}_5$  ( $\text{M} = \text{Cu}$ ,  $\text{Ni}$ ,  $\text{Co}$ ,  $\text{Fe}$ ,  $\text{Te}$ , and  $\text{Sb}$ ) are evaluated in Fig. 2(e) and (f), while the competing phase at each composition is listed in Table S2 (ESI<sup>†</sup>). In general, it can be inferred from Fig. 2(e) that all compounds have  $E_{\text{hull}}$  values increasing rapidly after intercalation from  $\text{Li}_3\text{M}_2\text{O}_5$ . For example,  $\text{Li}_3\text{V}_2\text{O}_5$  starts with an  $E_{\text{hull}}$  value of 21.02 meV per atom and then climbs to 190.28 meV per atom at the state of  $\text{Li}_5\text{V}_2\text{O}_5$ .



All other compounds in general have the same trend as  $\text{Li}_5\text{V}_2\text{O}_5$ . In contrast, for compounds with high voltage in Fig. 2(f), there is no clear trend of  $E_{\text{hull}}$  values. Particularly, the  $E_{\text{hull}}$  value of  $\text{Li}_{3+x}\text{Cu}_2\text{O}_5$  drops for Cu based system and the  $E_{\text{hull}}$  value of Sb based system first decreases and then increases during intercalation. There are also other systems, *i.e.*,  $\text{Li}_{3+x}\text{Co}_2\text{O}_5$ ,  $\text{Li}_{3+x}\text{Te}_2\text{O}_5$ , and  $\text{Li}_{3+x}\text{Ni}_2\text{O}_5$  based systems, showing similar  $E_{\text{hull}}$  values across all ranges of Li contents. Such divergent trends of  $E_{\text{hull}}$  values reveal potential fundamental differences in relative energies between low-voltage and high-voltage compounds. The correlation between relative energy among different lithiation states and average voltage will be explained more details in the discussion section.

As known to all, a promising DRX anode is expected to have positive voltage that is close to zero. As revealed by comparing Fig. 2(e) and (f), the average voltage seems to be correlated to relative energy among different lithiation states. From the definition of voltage, the actual potential is determined by the relative stability of at least two lithiated states, rather than the stability of a single composition (complete formula available in computational method). Moreover, it should be highlighted that the stability of overlithiated DRX is very sensitive to the metal ion radius, as well as the compatibility of specific metal ions in DRX structure,<sup>13</sup> regardless of the actual redox potential. Such feature further highlights the importance of relative stability as a descriptor for voltage rather than using the metal redox potential. The influence of relative stability on average voltage can be illustrated by the schematic in Fig. 3(a). By aligning the energy taking the pristine state  $\text{Li}_3\text{M}_2\text{O}_5$  as a reference, the relative energy of all other states  $\text{Li}_{3+x}\text{M}_2\text{O}_5$  ( $0 \leq x \leq 2$ ) can be illustrated by the y-axis in Fig. 3(a) as “relative energy”. Therefore, the slope of the plot indicates the chemical potential of Li in  $\text{Li}_{3+x}\text{M}_2\text{O}_5$  ( $0 \leq x \leq 2$ ). In other words, a more negative slope indicates a higher average voltage during the intercalation process.

The optimal voltage can be achieved by controlling the relative stability below and close to the black dash color as shown in Fig. 3(a), which corresponds to the chemical potential of Li metal. When the relative energy is too high for overlithiated DRX with respect to typical DRX (indicated with red arrow), the

intercalation will not happen given Li has a higher chemical potential than Li metal. When overlithiated DRX is overly stabilized compared to typical DRX (indicated with yellow arrow), or when the relative energy is too low, the average voltage will be too high to be a good anode. If the average voltage is high enough, such overlithiated DRX may be good cathode candidates. As a result, the optimal range of relative energy can be represented by the green arrow in Fig. 3(a). The real data of selected chemical systems are plotted in Fig. 3(b). Two overlithiated DRX materials are selected for each group, *e.g.*, negative, low positive voltage, and high positive voltage, respectively. The exact computed average voltage is shown as legend, which confirms that a more negative slope implies a higher average voltage during the intercalation process.

To further assess the practical application of the identified overlithiated DRX  $\text{Li}_{3+x}\text{M}_2\text{O}_5$  anodes, the energy density, phase stability, electronic conductivity, maximum volume change, and cost as estimated for five promising systems. A direct comparison across different metal chemistry is presented in Fig. 4 and more details are provided in Fig. S7 (ESI†). Particularly, the band gap is calculated with Heyd-Scuseria-Ernzerhof (HSE06) level of theory.<sup>26–28</sup> The lower band gap is used as a proxy for better electronic conductivity. To evaluate the pros and cons of several promising candidates, Fig. 4(a) shows that energy density, stability, electronic conductivity, volumetric change, and cost are typically considered to optimize for a high-performance anode. The top five  $\text{Li}_{3+x}\text{M}_2\text{O}_5$  systems with the highest energy density are selected for detailed analysis. Such systems are  $\text{Li}_{3+x}\text{V}_2\text{O}_5$ ,  $\text{Li}_{3+x}\text{Cr}_2\text{O}_5$ ,  $\text{Li}_{3+x}\text{Nb}_2\text{O}_5$ ,  $\text{Li}_{3+x}\text{Mn}_2\text{O}_5$ , and  $\text{Li}_{3+x}\text{Fe}_2\text{O}_5$  respectively, which show  $930.22 \text{ Wh kg}^{-1}$ ,  $749.05 \text{ Wh kg}^{-1}$ ,  $711.60 \text{ Wh kg}^{-1}$ ,  $663.02 \text{ Wh kg}^{-1}$ , and  $519.74 \text{ Wh kg}^{-1}$  correspondently. In addition to the energy densities in Fig. 4(b), the energy above hull ( $E_{\text{hull}}$ ) values for  $\text{Li}_3\text{M}_2\text{O}_5$  are demonstrated in Fig. 4(c), the average band gaps are demonstrated in Fig. 4(d), maximum volume changes are shown in Fig. 4(e), and cost per kilogram is presented in Fig. 4(f).

It can be inferred that except for Nb, all other four systems show reasonable stability, considering that a typical DRX that can be synthesized with solid-state reaction has around 50 meV per atom of  $E_{\text{hull}}$  value<sup>29</sup> (Table S3, ESI†). On the other hand, Nb

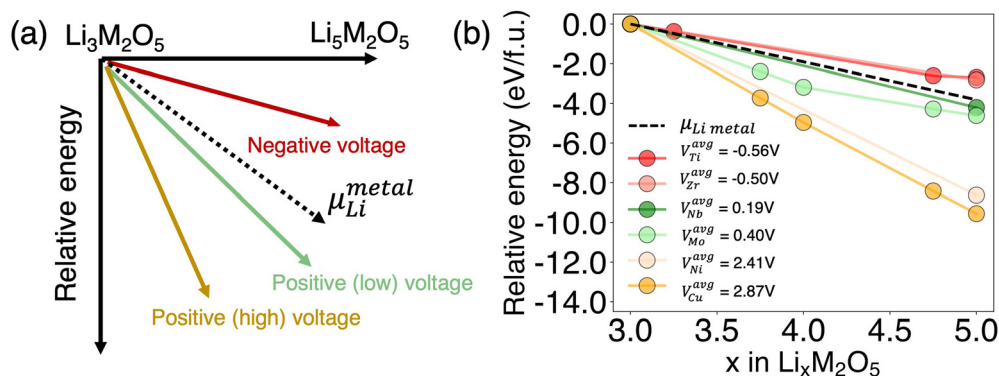


Fig. 3 (a) Schematic of three types of intercalation voltages with different trends of relative energy; (b) the computed relative voltage for selected DRX anode compositions  $\text{Li}_{3+x}\text{M}_2\text{O}_5$  ( $0 \leq x \leq 2$ ) ( $M = \text{Ti, Zr, Nb, Mo, Ni, and Cu}$ ).

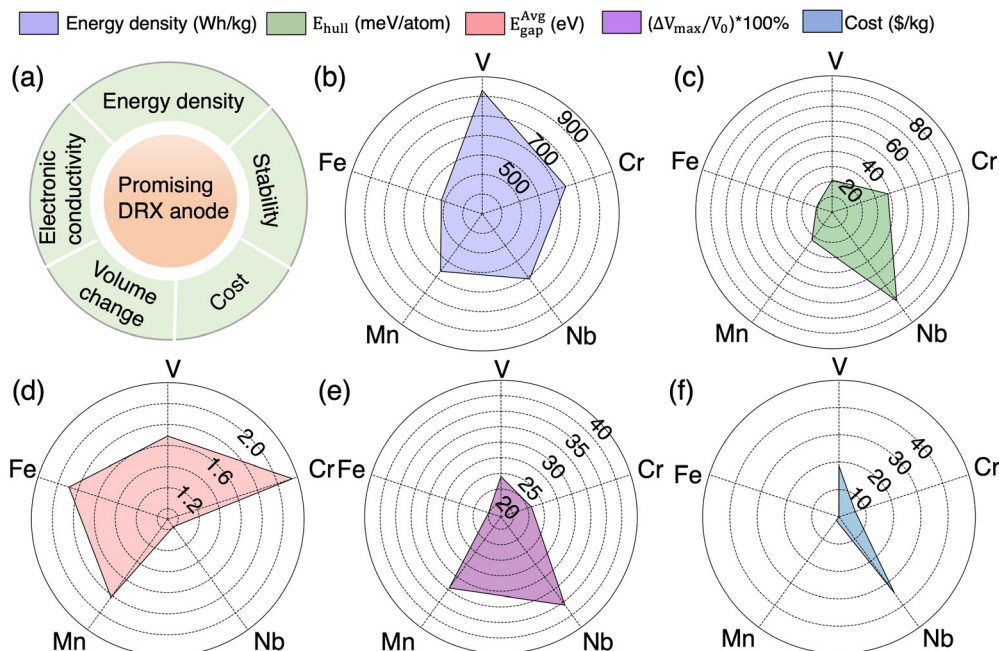


Fig. 4 (a) schematic of the typical metric to evaluate good anode, e.g., high energy density, good stability, good electronic conductivity, small volume change, and low cost; (b) the energy density, (c)  $E_{\text{hull}}$  of  $\text{Li}_{3+x}\text{M}_2\text{O}_5$ , (d) average band gap, (e) maximum volumetric change, and (f) cost of promising DRX  $\text{Li}_{3+x}\text{M}_2\text{O}_5$  ( $M = \text{V}, \text{Cr}, \text{Nb}, \text{Mn}, \text{and Fe}$ ).

based system seems to have extraordinary electronic conductivity than all other four systems due to a much smaller band gap of 0.99 eV compared with 1.69 eV, 2.15 eV, 1.82 eV, and 1.89 eV respectively. When comes to volumetric change, all five systems show much large volume change due to lithiation process, mainly because overlithiation tends to create short Li-metal bonds that forces the system to expand. The volume expansion percentage calculation of DRX  $\text{Li}_{3+x}\text{M}_2\text{O}_5$  is based on pristine  $\text{Li}_3\text{M}_2\text{O}_5$ . Among all five systems,  $\text{Li}_{3+x}\text{Fe}_2\text{O}_5$  seems to have the smallest value of maximum volume change during lithiation process, which is still substantial at 20.10%. Even though the volume change of all five overlithiated DRX anode systems is much larger than typical cathodes,<sup>30,31</sup> it is still close to the range of 13–30% volume change of carbon-based anodes<sup>32–34</sup> and much smaller compared to 300–400% volume change of silicon-based anodes.<sup>35–38</sup> With such consideration, the DRX anodes are quite reasonable in terms of volume change as anode materials. Furthermore, as the discovery of DRX-based anodes is still at its primary stage, it is also possible to further reduce the volume change or its impact by doping,<sup>39</sup> hierarchically structures design,<sup>40</sup> coating,<sup>41,42</sup> and solid electrolyte interphase (SEI) interface design.<sup>43</sup> Finally, it should be noted that  $\text{Li}_{3+x}\text{V}_2\text{O}_5$  and  $\text{Li}_{3+x}\text{Nb}_2\text{O}_5$  tend to be the most expensive systems in terms of cost in Fig. 4(f).

## Conclusions

In summary, 23 redox centers of overlithiated DRX  $\text{Li}_{3+x}\text{M}_2\text{O}_5$  were systematically evaluated for their voltage, theoretical capacity, energy density, phase stability, electronic conductivity, and volumetric change during cycling. The predicted DRX

$\text{Li}_{3+x}\text{V}_2\text{O}_5$ <sup>6</sup> has been experimentally reported. It displayed that DRX  $\text{Li}_{3+x}\text{V}_2\text{O}_5$  can be cycled reversibly between 0.01 V and 2 V with a specific capacity of  $\sim 255 \text{ mAh g}^{-1}$ , which is close to our calculated theoretical capacity of  $264.44 \text{ mAh g}^{-1}$  for  $\text{Li}_{3+x}\text{V}_2\text{O}_5$ . The reported experimental average voltage of 0.58 V for DRX  $\text{Li}_{3+x}\text{V}_2\text{O}_5$  is close to our calculated average voltage of 0.48 V. Therefore, the high-throughput DFT computations of DRX  $\text{Li}_{3+x}\text{M}_2\text{O}_5$  ( $0 \leq x \leq 2$ ) anode agree well with the reported experimental value. In addition to the explored  $\text{Li}_{3+x}\text{V}_2\text{O}_5$ ,  $\text{Li}_{3+x}\text{Nb}_2\text{O}_5$  system is shown as a promising anode system with low voltage, and high electronic conductivity, but its cost is higher and it's more challenging to synthesize.  $\text{Li}_{3+x}\text{Cr}_2\text{O}_5$  system also shows very competitive energy density and good rate performance in general, furthermore, there is no obvious disadvantage in terms of electronic conductivity, volume change, and price. Moreover, both  $\text{Li}_{3+x}\text{Fe}_2\text{O}_5$  and  $\text{Li}_{3+x}\text{Mn}_2\text{O}_5$  show reasonable performance as well. They have unique advantages being the cheapest transition metal on the periodic table. It is also worth noting that both Fe and Mn-based DRX systems show reasonable stability at various oxidation states. The energy density can be further increased by careful compositional optimization. It also revealed that the origin of the low voltage of DRX anode and proposed 'relative energy' to describe the correlation between voltage and phase stability of overlithiated DRX anode. The computed relative energies confirmed the principle that lithiated DRX should have reasonable stability to ensure low and positive average voltage. Therefore, this work provides compositional design principles for the new promising DRX anode of LIBs with high energy density, fast-charging capability, and good cycling stability.



## Computational methods

The high throughput density functional theory (DFT) calculations were carried out using the Vienna *ab initio* simulation package<sup>44</sup> and the projector-augmented wave (PAW) method,<sup>45,46</sup> with spin polarization consideration. A reciprocal mesh discretization of  $25 \text{ \AA}^{-1}$  has been used for each calculation. The threshold energy difference for electronic self-consistent convergence in the total free energy was set to  $1 \times 10^{-3} \text{ eV}$ . A plane wave energy cutoff of 520 eV was used for all calculations.  $\text{Li}_{3+x}\text{M}_2\text{O}_5$  structures are created with Li content ranging from 24 Li to 40 Li with M being one of the 23 selected metals. We derived all structures by creating partial occupancy through a rocksalt structure and then randomly sampling different ordered states with low electrostatic energies for DFT calculations and for constructing the convex hull. This method has been widely used in the past decades for battery calculations.<sup>47</sup> We also used the homemade script based on pymatgen<sup>48</sup> to automate all calculations and data processing. In addition, to evaluate the electronic conductivity of promising DRX  $\text{Li}_{3+x}\text{M}_2\text{O}_5$  ( $0 \leq x \leq 2$ ), the band gap is calculated with the implementation of the HSE (Heyd–Scuseria–Ernzerhof) exchange–correlation functional.<sup>26,27</sup> The band gap calculation is tested with different *K*-point densities. We found that the computed band gap values converge after using a  $15 \text{ \AA}^{-1}$  density of larger value. Therefore, all band gap calculations using HSE with  $15 \text{ \AA}^{-1}$  *K* mesh.

The theoretical capacity of all DRX is calculated within the effective lithiation/delithiation range. The formula of theoretical capacity is as follows:<sup>23</sup>

$$C_{\text{Theory}} = \frac{F \times n}{3.6 \times M}$$

where *F* is the Faraday constant, *n* is the number of electron transfers, and *M* represents the molar mass ( $\text{g mol}^{-1}$ ) of  $\text{Li}_3\text{M}_2\text{O}_5$ .

The volume changes are calculated on the structures on the intercalation convex hull. When quantifying voltage, energy density, relative energy, and the volume change of DRX  $\text{Li}_{3+x}\text{M}_2\text{O}_5$  ( $0 \leq x \leq 2$ ), the pristine  $\text{Li}_3\text{M}_2\text{O}_5$  is used as a reference.

The voltage of DRX  $\text{Li}_{3+x}\text{M}_2\text{O}_5$  ( $0 \leq x \leq 2$ ) during lithiation/delithiation can be expressed as follows:<sup>23</sup>

$$V = -(E(\text{Li}_{3+x}\text{M}_2\text{O}_5) - E(\text{Li}_3\text{M}_2\text{O}_5) - \mu_{\text{Li}}x)/x \quad (0 \leq x \leq 2)$$

where  $E(\text{Li}_{3+x}\text{M}_2\text{O}_5)$  is the total energy of  $\text{Li}_{3+x}\text{M}_2\text{O}_5$  per formula unit,  $E(\text{Li}_3\text{M}_2\text{O}_5)$  is the total energy of  $\text{Li}_3\text{M}_2\text{O}_5$  per formula unit, and  $\mu_{\text{Li}}$  is the chemical potential of lithium-ion. After obtaining the average voltage of anode, the energy density of DRX  $\text{Li}_{3+x}\text{M}_2\text{O}_5$  ( $0 \leq x \leq 2$ ) anode-based batteries is then calculated as follows:

$$\text{Energy density} = C_{\text{Theory}} \times (V_{\text{cathode}} - V_{\text{anode}})$$

where  $C_{\text{Theory}}$  is the theoretical capacity within effective lithiation/delithiation range,  $V_{\text{cathode}}$  is the average voltage of reference cathode, and  $V_{\text{anode}}$  is the average voltage of DRX  $\text{Li}_{3+x}\text{M}_2\text{O}_5$  ( $0 \leq x \leq 2$ ) within positive voltage range during lithiation/delithiation. In this work, we considered one reference 4 V of Ni-rich cathodes ( $V_{\text{cathode}} = 4 \text{ V}$ ).

The correlation between voltage and relative structure stability is described by the relative energy. The relative energy formula of  $\text{Li}_{3+x}\text{M}_2\text{O}_5$  ( $0 \leq x \leq 2$ ) is as follows:

$$E_{\text{relative energy}} = E(\text{Li}_{3+x}\text{M}_2\text{O}_5) - E(\text{Li}_3\text{M}_2\text{O}_5) \quad (0 \leq x \leq 2)$$

where  $E(\text{Li}_{3+x}\text{M}_2\text{O}_5)$  is the total energy of  $\text{Li}_{3+x}\text{M}_2\text{O}_5$  per formula unit and  $E(\text{Li}_3\text{M}_2\text{O}_5)$  is the total energy of  $\text{Li}_3\text{M}_2\text{O}_5$  per formula unit. Therefore, from voltage and relative energy formulas, it is obvious that the relative energy term  $E_{\text{relative energy}}$  determines the theoretical average voltage. Physically, this can be understood as the stability of the metastable overlithiated state will determine the average voltage of the DRX  $\text{Li}_{3+x}\text{M}_2\text{O}_5$  ( $0 \leq x \leq 2$ ) when utilized as an anode.

## Data availability

The data that support the findings of this study are available from the author upon reasonable request.

## Conflicts of interest

The authors declare no competing interests.

## Acknowledgements

This work was supported by the startup funding from Florida State University. The Computational resources were provided by the Advanced Cyberinfrastructure Coordination Ecosystem: Services & Support (ACCESS), the National Energy Research Scientific Computing Center (NERSC), a DOE Office of Science User Facility supported by the Office of Science and the U.S. Department of Energy under contract no. DE-AC02-05CH11231 and Research Computing Center (RCC) at Florida State University. The computation and data processing were also supported by the supercomputing resources from the Department of Energy's Office of Energy Efficiency and Renewable Energy at the National Renewable Energy Laboratory.

## References

- 1 Y. Tian, G. Zeng, A. Rutt, T. Shi, H. Kim, J. Wang, J. Koettgen, Y. Sun, B. Ouyang and T. Chen, Promises and challenges of next-generation “beyond Li-ion” batteries for electric vehicles and grid decarbonization, *Chem. Rev.*, 2020, **121**(3), 1623–1669.
- 2 M. Armand and J.-M. Tarascon, Building better batteries, *Nature*, 2008, **451**(7179), 652–657.
- 3 A. Manthiram, An outlook on lithium ion battery technology, *ACS Cent. Sci.*, 2017, **3**(10), 1063–1069.
- 4 J. B. Goodenough and K.-S. Park, The Li-ion rechargeable battery: a perspective, *J. Am. Chem. Soc.*, 2013, **135**(4), 1167–1176.
- 5 M. S. Whittingham, Electrical energy storage and intercalation chemistry, *Science*, 1976, **192**(4244), 1126–1127.
- 6 H. Liu, Z. Zhu, Q. Yan, S. Yu, X. He, Y. Chen, R. Zhang, L. Ma, T. Liu and M. Li, A disordered rock salt anode for



- fast-charging lithium-ion batteries, *Nature*, 2020, **585**(7823), 63–67.
- 7 P. Barnes, Y. Zuo, K. Dixon, D. Hou, S. Lee, Z. Ma, J. G. Connell, H. Zhou, C. Deng and K. Smith, Electrochemically induced amorphous-to-rock-salt phase transformation in niobium oxide electrode for Li-ion batteries, *Nat. Mater.*, 2022, **21**(7), 795–803.
  - 8 X. Guo, C. Chen and S. P. Ong, Intercalation chemistry of the disordered rocksalt  $\text{Li}_3\text{V}_2\text{O}_5$  anode from cluster expansions and machine learning interatomic potentials, *Chem. Mater.*, 2023, **35**(4), 1537–1546.
  - 9 D. Mikhailova, A. Voss, S. Oswald, A. Tsirlin, M. Schmidt, A. Senyshyn, J. Eckert and H. Ehrenberg, Lithium insertion into  $\text{Li}_2\text{MoO}_4$ : reversible formation of  $\text{Li}_3\text{MoO}_4$  with a disordered rock-salt structure, *Chem. Mater.*, 2015, **27**(12), 4485–4492.
  - 10 R. Clément, Z. Lun and G. Ceder, Cation-disordered rocksalt transition metal oxides and oxyfluorides for high energy lithium-ion cathodes, *Energy Environ. Sci.*, 2020, **13**(2), 345–373.
  - 11 A. R. Armstrong, C. Lyness, P. M. Panchmatia, M. S. Islam and P. G. Bruce, The lithium intercalation process in the low-voltage lithium battery anode  $\text{Li}_{1+x}\text{V}_{1-x}\text{O}_2$ , *Nat. Mater.*, 2011, **10**(3), 223–229.
  - 12 Y. Qin, H. Zhao, M. Hua, J. Gao, J. Lu, S. Zhang, X. Lin, J. Sun, L. Yin and R. Wang, Pseudocapacitive lithium-rich disordered rock salt vanadium oxide with 3D lithium-ion transport pathways for high-performance lithium-ion capacitor, *J. Power Sources*, 2023, **588**, 233722.
  - 13 Y. Chen, Z. Lun, X. Zhao, K. P. Koirala, L. Li, Y. Sun, C. A. O'Keefe, X. Yang, Z. Cai and C. Wang, Unlocking Li superionic conductivity in face-centred cubic oxides *via* face-sharing configurations, *Nat. Mater.*, 2024, 1–8.
  - 14 Z. Jadidi, T. Chen, L. Barroso-Luque and G. Ceder, Kinetics of Li transport in vanadium-based disordered rocksalt structures, *Chem. Mater.*, 2023, **35**(21), 9225–9234.
  - 15 W. Zhang, D.-H. Seo, T. Chen, L. Wu, M. Topsakal, Y. Zhu, D. Lu, G. Ceder and F. Wang, Kinetic pathways of ionic transport in fast-charging lithium titanate, *Science*, 2020, **367**(6481), 1030–1034.
  - 16 H. Ji, J. Wu, Z. Cai, J. Liu, D.-H. Kwon, H. Kim, A. Urban, J. K. Papp, E. Foley and Y. Tian, Ultrahigh power and energy density in partially ordered lithium-ion cathode materials, *Nat. Energy*, 2020, **5**(3), 213–221.
  - 17 F. N. U. Khan, M. G. Rasul, A. Sayem and N. Mandal, Maximizing energy density of lithium-ion batteries for electric vehicles: a critical review, *Energy Rep.*, 2023, **9**, 11–21.
  - 18 C. Wang, C. Yang and Z. Zheng, Toward practical high-energy and high-power lithium battery anodes: present and future, *Adv. Sci.*, 2022, **9**(9), 2105213.
  - 19 Y. Son, T. Lee, B. Wen, J. Ma, C. Jo, Y.-G. Cho, A. Boies, J. Cho and M. De Volder, High energy density anodes using hybrid Li intercalation and plating mechanisms on natural graphite, *Energy Environ. Sci.*, 2020, **13**(10), 3723–3731.
  - 20 B. Zhu, X. Wang, P. Yao, J. Li and J. Zhu, Towards high energy density lithium battery anodes: silicon and lithium, *Chem. Sci.*, 2019, **10**(30), 7132–7148.
  - 21 I. Beyers, A. Bensmann and R. Hanke-Rauschenbach, Ragone plots revisited: a review of methodology and application across energy storage technologies, *J. Energy Storage*, 2023, **73**, 109097.
  - 22 J. Woods, A. Mahvi, A. Goyal, E. Kozubal, A. Odukomaiya and R. Jackson, Rate capability and Ragone plots for phase change thermal energy storage, *Nat. Energy*, 2021, **6**(3), 295–302.
  - 23 L. Wang, J. Wang and B. Ouyang, Computational Investigation of MAX as Intercalation Host for Rechargeable Aluminum-Ion Battery, *Adv. Energy Mater.*, 2023, **13**(46), 2302584.
  - 24 H. Liu, Z. Xie, W. Qu, E. Dy, S. Niketic, S. Brueckner, K. Tsay, E. Fuller, C. Bock and N. Zaker, High-voltage induced surface and intragranular structural evolution of Ni-rich layered cathode, *Small*, 2022, **18**(19), 2200627.
  - 25 L. David, D. Mohanty, L. Geng, R. E. Ruther, A. S. Sefat, E. Cakmak, G. M. Veith, H. M. Meyer III, H. Wang and D. L. Wood III, High-Voltage Performance of Ni-Rich NCA Cathodes: Linking Operating Voltage with Cathode Degradation, *ChemElectroChem*, 2019, **6**(22), 5571–5580.
  - 26 J. Heyd and G. E. Scuseria, Efficient hybrid density functional calculations in solids: assessment of the Heyd-Scuseria-Ernzerhof screened Coulomb hybrid functional, *J. Chem. Phys.*, 2004, **121**(3), 1187–1192.
  - 27 J. Heyd, J. E. Peralta, G. E. Scuseria and R. L. Martin, Energy band gaps and lattice parameters evaluated with the Heyd-Scuseria-Ernzerhof screened hybrid functional, *J. Chem. Phys.*, 2005, **123**(17), 174101.
  - 28 D.-H. Seo, A. Urban and G. Ceder, Calibrating transition-metal energy levels and oxygen bands in first-principles calculations: accurate prediction of redox potentials and charge transfer in lithium transition-metal oxides, *Phys. Rev. B: Condens. Matter Mater. Phys.*, 2015, **92**(11), 115118.
  - 29 H. Ji, A. Urban, D. A. Kitchaev, D.-H. Kwon, N. Artrith, C. Ophus, W. Huang, Z. Cai, T. Shi and J. C. Kim, Hidden structural and chemical order controls lithium transport in cation-disordered oxides for rechargeable batteries, *Nat. Commun.*, 2019, **10**(1), 592.
  - 30 X. Zhao, Y. Tian, Z. Lun, Z. Cai, T. Chen, B. Ouyang and G. Ceder, Design principles for zero-strain Li-ion cathodes, *Joule*, 2022, **6**(7), 1654–1671.
  - 31 X. Zhao and G. Ceder, Zero-strain cathode materials for Li-ion batteries, *Joule*, 2022, **6**(12), 2683–2685.
  - 32 S. Schweidler, L. de Biasi, A. Schiele, P. Hartmann, T. Brezesinski and J. Janek, Volume changes of graphite anodes revisited: a combined operando X-ray diffraction and in situ pressure analysis study, *J. Phys. Chem. C*, 2018, **122**(16), 8829–8835.
  - 33 K. Dai, Z. Wang, G. Ai, H. Zhao, W. Yuan, X. Song, V. Battaglia, C. Sun, K. Wu and G. Liu, The transformation of graphite electrode materials in lithium-ion batteries after cycling, *J. Power Sources*, 2015, **298**, 349–354.
  - 34 N. Kobayashi, Y. Inden and M. Endo, Silicon/soft-carbon nanohybrid material with low expansion for high capacity and long cycle life lithium-ion battery, *J. Power Sources*, 2016, **326**, 235–241.



- 35 H. Schmidt, B. Jerliu, E. Hüger and J. Stahn, Volume expansion of amorphous silicon electrodes during potentiostatic lithiation of Li-ion batteries, *Electrochem. Commun.*, 2020, **115**, 106738.
- 36 B. Jerliu, E. Huger, L. Dorrer, B.-K. Seidlhofer, R. Steitz, V. Oberst, U. Geckle, M. Bruns and H. Schmidt, Volume expansion during lithiation of amorphous silicon thin film electrodes studied by in-operando neutron reflectometry, *J. Phys. Chem. C*, 2014, **118**(18), 9395–9399.
- 37 C. R. Becker, K. E. Strawhecker, Q. P. McAllister and C. A. Lundgren, In situ atomic force microscopy of lithiation and delithiation of silicon nanostructures for lithium ion batteries, *ACS Nano*, 2013, **7**(10), 9173–9182.
- 38 C. Cao, H.-G. Steinrück, B. Shyam, K. H. Stone and M. F. Toney, In situ study of silicon electrode lithiation with X-ray reflectivity, *Nano Lett.*, 2016, **16**(12), 7394–7401.
- 39 S. Hoshino, A. M. Glushenkov, S. Ichikawa, T. Ozaki, T. Inamasu and N. Yabuuchi, Reversible three-electron redox reaction of  $\text{Mo}^{3+}/\text{Mo}^{6+}$  for rechargeable lithium batteries, *ACS Energy Lett.*, 2017, **2**(4), 733–738.
- 40 K. X. Wang, X. H. Li and J. S. Chen, Surface and interface engineering of electrode materials for lithium-ion batteries, *Adv. Mater.*, 2015, **27**(3), 527–545.
- 41 K. Du, A. Gao, L. Gao, S. Sun, X. Lu, C. Yu, S. Li, H. Zhao and Y. Bai, Enhancing the structure stability of Ni-rich  $\text{LiNi}_{0.6}\text{Co}_{0.2}\text{Mn}_{0.2}\text{O}_2$  cathode via encapsulating in negative thermal expansion nanocrystalline shell, *Nano Energy*, 2021, **83**, 105775.
- 42 C. Zhao, C. Wang, X. Liu, I. Hwang, T. Li, X. Zhou, J. Diao, J. Deng, Y. Qin and Z. Yang, Suppressing strain propagation in ultrahigh-Ni cathodes during fast charging via epitaxial entropy-assisted coating, *Nat. Energy*, 2024, **9**(3), 345–356.
- 43 C. Cui, X. Fan, X. Zhou, J. Chen, Q. Wang, L. Ma, C. Yang, E. Hu, X.-Q. Yang and C. Wang, Structure and interface design enable stable Li-rich cathode, *J. Am. Chem. Soc.*, 2020, **142**(19), 8918–8927.
- 44 J. Hafner and G. Kresse, The vienna *ab initio* simulation program VASP: an efficient and versatile tool for studying the structural, dynamic, and electronic properties of materials, *Properties of Complex Inorganic Solids*, Springer, 1997, pp. 69–82.
- 45 J. P. Perdew, K. Burke and M. Ernzerhof, Generalized gradient approximation made simple, *Phys. Rev. Lett.*, 1996, **77**(18), 3865.
- 46 G. Kresse and J. Furthmüller, Efficient iterative schemes for *ab initio* total-energy calculations using a plane-wave basis set, *Phys. Rev. B: Condens. Matter Mater. Phys.*, 1996, **54**(16), 11169.
- 47 A. Urban, D.-H. Seo and G. Ceder, Computational understanding of Li-ion batteries, *npj Comput. Mater.*, 2016, **2**(1), 1–13.
- 48 S. P. Ong, W. D. Richards, A. Jain, G. Hautier, M. Kocher, S. Cholia, D. Gunter, V. L. Chevrier, K. A. Persson and G. Ceder, Python Materials Genomics (pymatgen): a robust, open-source python library for materials analysis, *Comput. Mater. Sci.*, 2013, **68**, 314–319.

